Research Article | Open Access

Soft Science

Li *et al*. *Soft Sci*. **2026**, *6*, 39 **DOI:**10.20517/ss.2026.18

Actuation-sensing coupled plasmonic microrobots for adsorption-mediated chemical detection

Ruyu Li[1], Zhuo-Chen Ma[2,3,*], Ruokun He[2], Yunlang Zhou[2], Zihan Luo[1], Yuntian Du[1], Jienan Wang[4], Yueqi Zhu[4], Hesheng Wang[2], Bing Han[1,3,*]

Keywords:
Femtosecond laser direct writing, magnetic soft robot, surface-enhanced Raman scattering, conformal integration, *in situ* sensing

Citation: Li, R.; Ma, Z. C.; He, R.; Zhou, Y.; Luo, Z.; Du, Y.; Wang, J.; Zhu, Y.; Wang, H.; Han, B. Actuation-sensing coupled plasmonic microrobots for adsorption-mediated chemical detection. *Soft Sci.* **2026**, *6*, 39. https://dx.doi.org/10.20517/ss.2026.18

Received: 27 Jan 2026
First Decision: 10 Mar 2026
Revised: 24 Mar 2026
Accepted: 8 Apr 2026
Published: 20 May 2026

Academic Editor:
Zhigang Wu
Copy Editor:
Shu-Yuan Duan
Production Editor:
Shu-Yuan Duan

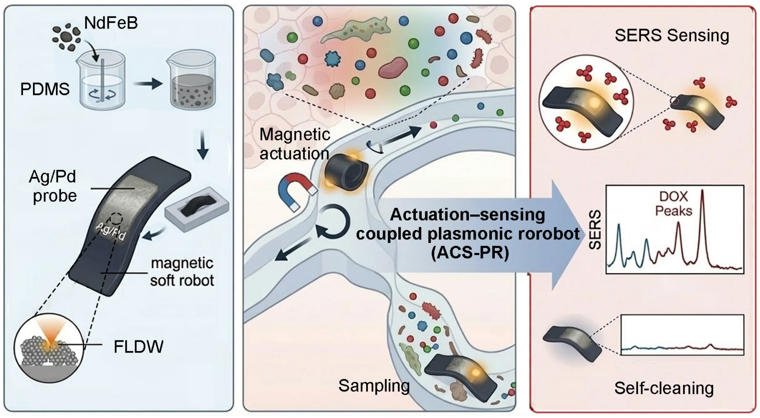

Abstract

Chemical sensing at small scales is essential for obtaining ultrasensitive and molecularly specific readouts of complex biological microenvironments. However, sensing probes, such as surface-enhanced Raman scattering (SERS), remain predominantly limited to static substrates or freely dispersed nanoparticles with poor spatial controllability, retrievability and long-term stability. Consequently, effective coupling between SERS sensing and robotic actuation has yet to be achieved. Here we introduce a magnetically steerable MagSense-Bot that enables hot-spots-on-the-fly SERS sensing and establishes an Actuation-Sensing Coupled Plasmonic Robotics (ASC-PR) framework. Plasmonic hot spots are deterministically integrated with milli-robot magnetic actuation, allowing SERS sensing interfaces to be actively transported, positioned and oriented for spatially addressable chemical interrogation. This capability is enabled by femtosecond-laser-based conformal integration of chemically robust Ag-Pd alloy nanostructures onto curved robotic bodies, ensuring stable plasmonic performance under biologically relevant conditions. We

---

[1]School of Biomedical Engineering, Shanghai Jiao Tong University, Shanghai 200240, China.
[2]School of Automation and Intelligent Sensing, Shanghai Jiao Tong University, Shanghai 200240, China.
[3]Institute of Medical Robotics, Shanghai Jiao Tong University, Shanghai 200240, China.
[4]Department of Radiology, Shanghai Sixth People's Hospital Affiliated to Shanghai Jiao Tong University School of Medicine, Shanghai 200233, China.

[*]**Correspondence to:** Prof. Bing Han, School of Biomedical Engineering, Shanghai Jiao Tong University, Shanghai 200240, China. E-mail: binghan@sjtu.edu.cn; Prof. Zhuo-Chen Ma, School of Automation and Intelligent Sensing, Shanghai Jiao Tong University, Shanghai 200240, China. E-mail: zcma@sjtu.edu.cn

demonstrate the concept through *in situ* SERS probing of doxorubicin (DOX) within tumor-mimicking microenvironments, illustrating that actuation-controlled mobile hot spots can access localized chemical information beyond the reach of static or non-retrievable probes. By effectively coupling plasmonic sensing with magnetic milli-robot actuation, this work redefines small-scale robots as active chemical interrogators and opens new opportunities for *in situ* molecular analysis in confined and heterogeneous systems.

INTRODUCTION

Chemical sensing plays a pivotal role in biomedical diagnostics[1-4], therapeutic monitoring, and the investigation of complex biochemical processes[5,6]. In many biological systems, particularly in tumors and diseased tissues, chemical information is highly localized, dynamically evolving and strongly heterogeneous across space and time. Capturing such information therefore requires sensing techniques that are not only sensitive, but also capable of resolving molecular signatures at specific locations. Surface-enhanced Raman scattering (SERS) has emerged as a powerful chemical sensing technique owing to its ultrahigh sensitivity and intrinsic molecular fingerprinting capability[7-11]. By amplifying Raman signals through localized plasmonic fields, SERS enables label-free identification of chemical species at low concentrations, making it attractive for *in situ* biochemical analysis in complex biological environments. Despite these advantages, most existing SERS sensing platforms are fundamentally static. Current implementations typically rely on planar substrates[12], rigid probes[13], or freely dispersed plasmonic nanoparticles[14], which are commonly fabricated by lithography[15], chemical synthesis[16], or self-assembly[17]. While these approaches have enabled sensitive detection under controlled conditions, they impose inherent limitations when deployed *in vivo* or in confined biological environments. SERS platforms typically rely on static substrates, which lack spatial controllability, are often suffer from signal instability and material degradation *in vivo*. Freely injected nanoparticles, although mobile, cannot be deterministically positioned, may diffuse uncontrollably, and raise concerns regarding leakage, accumulation and long-term biosafety. Therefore, we need a reliable and spatially addressable SERS sensing platform which can effectively function in complex biological microenvironments.

Recent advances in soft robotics and small-scale robotic systems have opened new opportunities for biomedical applications, including targeted drug delivery[18], minimally invasive surgery[19], and local therapeutic intervention[20,21]. In particular, milli-robots actuated by external magnetic fields have demonstrated sophisticated locomotion modes (such as rolling, crawling, swimming and shape morphing)[22-25] enabling navigation through confined and tortuous biological spaces under low Reynolds number conditions[26-29]. These magnetically actuated milli-robots have been explored for a range of medical tasks, including vascular navigation[30], thrombus removal and localized therapy[31]. For example, Zhu *et al.* developed a bionic blood-gel magnetic soft milli-robot capable of multimodal locomotion under a programmable external magnetic field[32]. Notably, the robot demonstrated effective navigation within the cerebrospinal fluid environment of the extremely confined subarachnoid space. Assisted by X-ray imaging guidance, the system enabled precise, noninvasive access to intracranial tumor regions, achieving targeted drug delivery, which opens up a new path for the precise and non-invasive treatment of deep intracranial tumors and adjacent functional areas. Similarly, Xu *et al.* also developed a bionic magnetic soft robot inspired by the golden wheel spider[33]. Owing to its unique structural design and magnetic actuation, the robot exhibited robust locomotion across arbitrarily inclined and even inverted surfaces, successfully overcoming mucus-rich environments and vertical obstacles with height differences of up to 8 cm. When integrated with real-time visual feedback and magnetic control, this platform demonstrated versatile mobility across multiple organs, offering a compelling approach for targeted drug delivery and minimally invasive surgical interventions. However, despite their impressive mobility and controllability, their potential to perform high-information chemical sensing has remained largely unrealized. Existing robotic platforms are predominantly designed as actuators or carriers, while chemical sensing with molecularly specific sensitivity remains absent.

Herein, we introduce MagSense-Bot, a magnetically steerable milli-robot that establishes an Actuation-Sensing Coupled Plasmonic Robotics (ASC-PR) paradigm. When combined with magnetically actuated milli-robots capable of navigating confined biological spaces, SERS sensors gain controlled mobility, enabling them to function as "hot-spots-on-the-fly" rather than static or passively dispersed probes [Supplementary Table 1]. By utilizing femtosecond-laser-enabled conformal fabrication[34-36], plasmonic Ag-Pd alloy nanostructures are directly integrated onto the curved robotic surface, allowing precise spatial patterning and strong structural-material synergy. The composite alloy significantly enhances chemical robustness against oxidation and biofouling, ensuring reliable SERS sensing performance in complex tumor micro-environments where conventional Ag-based hot spots rapidly degrade. This integration strategy bridges precision laser micro/nanofabrication with robotic systems, enabling stable plasmonic sensing beyond planar substrates. As a proof of concept, MagSense-Bot is employed for active, *in situ* SERS detection of doxorubicin (DOX) within tumor microenvironments, demonstrating the ability to probe drug-related chemical signatures at specific locations inaccessible to static probes or passive sensing approaches. This capability highlights the potential of mobile SERS hot spots for investigating spatial heterogeneity in drug distribution and microenvironment interactions.

EXPERIMENTAL

Characterization

Scanning electron microscopy (SEM) and energy-dispersive X-ray spectroscopy (EDS) were performed using a field-emission SEM (JEOL JSM-7800F, Japan) operating at 15 kV. Atomic force microscopy (AFM) images were acquired in tapping mode using an MFP-3D system (Asylum Research, USA). Magnetic hysteresis loops were measured using a magnetic property measurement system (MPMS3, Quantum Design, USA). Optical images were obtained with an upright optical microscope (Mshot, MJ43, China). Contact angle measurements were carried out using a Theta Flex goniometer (Biolin, Scientific, Sweden). Fluorescence imaging was performed using an inverted fluorescence microscope (Keyence, BZ-X800, Japan).

Femtosecond-laser fabrication of Ag/Pd alloy

Ag and Pd precursor solutions were prepared by complexing $AgNO_3$ or $PdCl_2$ (0.1 M) with sodium citrate (0.1 M) in ammonia-containing aqueous solutions until clear and homogeneous. The two precursor solutions were then mixed at a predefined volume ratio to obtain the Ag/Pd mixed precursor. Ag/Pd alloy microstructures were directly patterned on flexible substrates using a femtosecond laser direct writing (FLDW) system (Maleon, JC-Ultrafast, China, Equipment, 800 nm wavelength, 100 fs pulse duration, 80 MHz repetition rate) equipped with a 60× objective (NA = 1.42, Nikon, Japan). The laser power and exposure time were set to 10 mW and 50 μs, respectively, with all processing steps controlled by computer-defined scanning. The laser power reported in this work was measured before the objective lens using a calibrated optical power meter. After fabrication, samples were rinsed with deionized water to remove residual precursors and dried under nitrogen.

Fabrication of the magnetic soft robot

The magnetic soft small-scale robots were fabricated using a template-assisted magnetization strategy [Supplementary Text 1]. PDMS and NdFeB particles were blended at a 1:1 mass ratio and spin-coated onto a pre-cleaned glass substrate, followed by thermal curing for 6 h. Subsequently, an infrared laser was utilized to precisely cut the cured composite into the designed geometries. Finally, the fabricated robots were shaped using a 3D-printed mold and subjected to programmable magnetization with a magnetizer (Shenzhen Jiuju Industrial Equipment, MA 2030, China).

FDTD simulation

The electric field distribution was simulated using the finite-difference time-domain (FDTD) method. Nanoparticles with an average diameter of approximately 50 nm and an interparticle spacing of 10 nm were used to represent the plasmonic hot-spot configuration. The Ag/Pd alloy (molar ratio of 4:1) was modeled using the Bruggeman effective medium approximation, with dielectric functions of Ag and Pd taken from the Johnson-Christy and Palik datasets, respectively. The effective permittivity was obtained by solving the Bruggeman equation[37,38]:

$$f_{Ag}\frac{\varepsilon_{Ag}-\varepsilon_{\mathrm{eff}}}{\varepsilon_{Ag}+2\varepsilon_{\mathrm{eff}}}+f_{pd}\frac{\varepsilon_{pd}-\varepsilon_{\mathrm{eff}}}{\varepsilon_{pd}+2\varepsilon_{\mathrm{eff}}}=0 \tag{1}$$

where the volume fractions were set to $f_{Ag} = 0.8$ and $f_{pd} = 0.2$. The resulting dispersion curve $\varepsilon_{eff}(\omega)$ was imported as a user-defined material in the FDTD solver.

COMSOL simulation

To understand the programmable deformation of the magnetic soft robot, finite-element simulations were performed using a coupled magneto-elastic model. The magnetized segments were treated as hard-magnetic domains embedded in an elastic matrix. The magnetic torque acting on each segment was calculated as $T = m \times B$ where m is the programmed magnetization vector and B is the applied magnetic field.

The simulations were conducted using COMSOL Multiphysics. The magnetic elastomer was modeled as a linear elastic material with a remanent magnetization of 2.4×10^5 A m^{-1} and a Young's modulus of 1.23 MPa. The magnetization of each arm followed the N-S polarity pattern. Under a 20 mT magnetic field, adjacent arms experienced opposite magnetic torques, leading to symmetric out-of-plane bending consistent with the experimental observations.

SERS signal detection of R6G/CV

Raman measurements were performed using a confocal Raman spectrometer (Renishaw, UK) equipped with a 532 nm laser. The laser power at the sample was 2 mW, with an integration time of 10 s and 3 accumulations per spectrum. A 50× objective lens was used throughout the experiments.

Magnetic control system

A custom-built magnetic control system was employed to actuate the MagSense-Bot, consisting of a triaxial Helmholtz coil (Hunan Payson Technology, PS-3HM340, China) driven by a three-channel waveform generator (FeelElec, FY8300S, China) and power amplifiers (Hunan Payson Technology, PS-GL5050, China). Independently controlled signals applied to each coil axis generated programmable three-dimensional magnetic fields for precise robotic actuation. The locomotion behaviors of the magnetic robot were recorded and analyzed using an optical imaging system (Riel Vision Technology, MIX317, China) [Supplementary Figure 1]. The robot was actuated by an external magnetic field with a field strength of 20 mT and an actuation frequency ranging from 0 to 50 Hz, depending on the specific experiment. For clarity, the exact field and frequency used in each experiment are also indicated in the corresponding figure captions/text.

Biocompatibility assessment

Human fibroblasts obtained from Beyotime Biotechnology (Shanghai, China) were used to assess the cytotoxicity of the magnetic robots. The robot samples were sterilized by ultraviolet irradiation sterilization and placed individually into the wells of a 6-well culture plate. The cell suspensions were then seeded into each well. All samples were prepared in triplicate and incubated for 36 h. Following incubation, the cells were stained with a Calcein-AM/PI double-staining kit and examined under a fluorescence microscope.

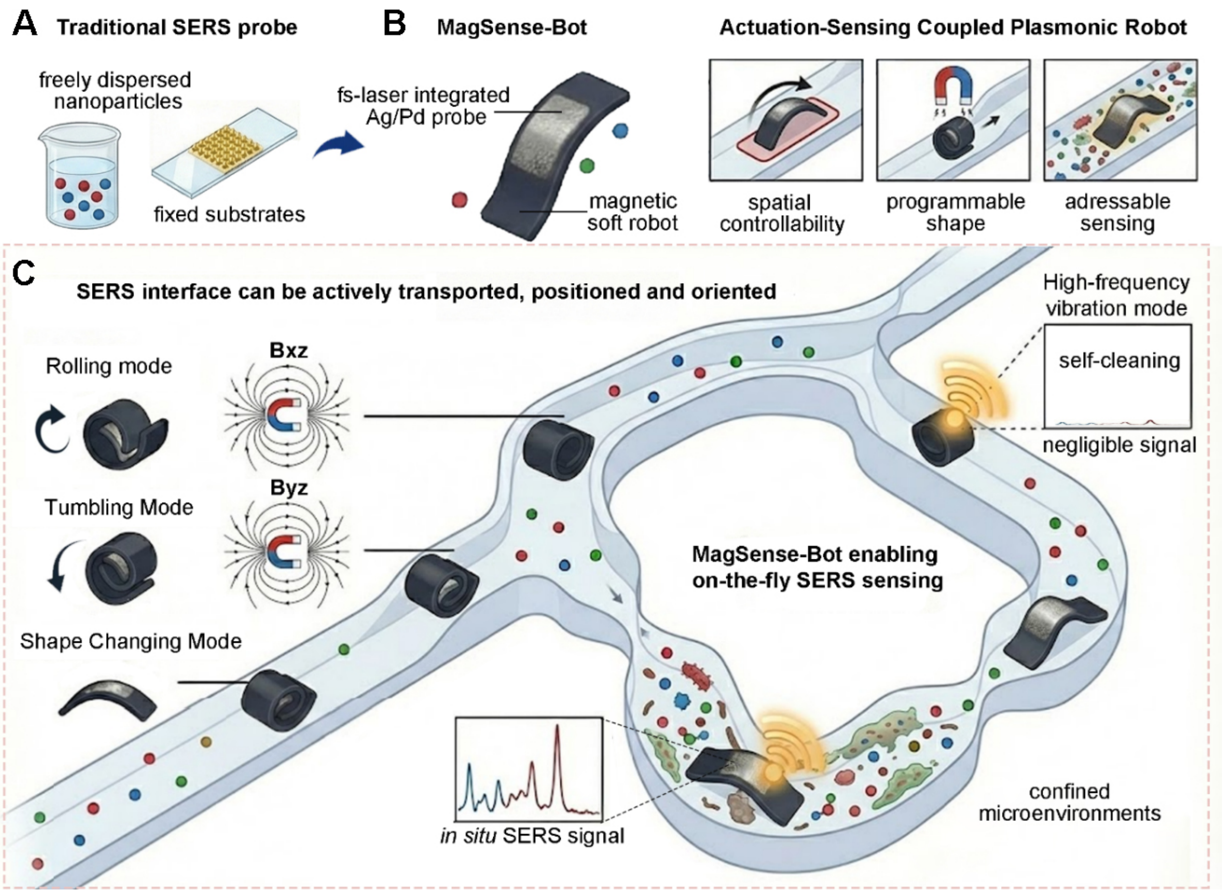

Figure 1. Schematic illustration comparing conventional SERS sensing platforms and the proposed ASC-PR paradigm. (A) Traditional SERS probes; (B) Design of a the MagSense-Bot and its merits; (C) Actuation-sensing coupled plasmonic robot system that can realize active navigation and localized chemical interrogation. SERS: Surface-enhanced Raman scattering; ASC-PR: Actuation-Sensing Coupled Plasmonic Robotics.

RESULTS AND DISCUSSION

Concept and design of Actuation-Sensing Coupled Plasmonic Robotics

Conventional SERS-based chemical probes are predominantly realized in two forms [Figure 1A]: freely dispersed plasmonic nanoparticles and fixed plasmonic substrates. Dispersed nanoparticles offer high surface accessibility and strong signal enhancement, however, their uncontrolled diffusion, potential accumulation, and poor retrievability severely restrict their use for site-specific chemical interrogation within confined or heterogeneous biological lesions. Besides, planar or fixed SERS substrates provide improved structural stability but are intrinsically limited to predefined locations, rendering them unsuitable for probing buried, irregularly shaped, or dynamically evolving pathological regions. The lack of a controllable and retrievable carrier makes the delivery of plasmonic sensing interfaces to designated locations within complex biological environments a fundamental bottleneck. Addressing this challenge requires not merely improving plasmonic materials, but rethinking how and where SERS sensing interfaces operate.

We propose integrating plasmonic SERS nanostructures directly onto the surface of a soft magnetic robot, namely MagSense-Bot [Figure 1B], thereby transforming static or passively distributed SERS probes into an actively maneuverable sensing system. By leveraging the advanced locomotion capabilities of magnetically actuated milli-robots, plasmonic sensing elements can be flexibly delivered to confined spaces and precisely positioned at targeted lesion sites. More importantly, the compliant nature of soft robots allows conformal contact with biological surfaces of arbitrary geometry, enhancing interfacial interaction between SERS hot spots and target analytes and improving detection efficiency in irregular microenvironments. This emerging class of systems is defined as Actuation-Sensing Coupled Plasmonic Robotics (ASC-PR), in which plasmonic sensing interfaces are deterministically integrated with and actively repositioned by robotic actuation, enabling spatially addressable and site-specific chemical interrogation.

Magnetic actuation plays a central role in enabling ASC-PR [Figure 1C]. Under externally applied alternating, rotating, or gradient magnetic fields, soft magnetic robots can be driven with multiple degrees of freedom across the *xy*, *xz*, and *yz* planes, allowing precise control over both translational motion and orientation. Moreover, programmable magnetic fields enable dynamic modulation of the robot's overall configuration: in a compact state, the robot can navigate through narrow and tortuous passages, while in an expanded or deformed state, the plasmonic sensing interface can be deployed over a larger effective area to maximize analyte capture at the target site. Beyond spatial positioning, magnetic actuation also introduces functional dynamics at the sensing interface. Periodic magnetic excitation can induce controlled deformation or vibration of the plasmonic surface, facilitating high-frequency removal of nonspecifically adsorbed molecules. This self-cleaning capability enables repeated sensing cycles during a single deployment, allowing one-time delivery followed by multiple localized measurements, thereby reducing repeated insertion, shortening operational time, and minimizing procedural disturbance.

Through this actuation-sensing coupled design, plasmonic SERS hot spots acquire mobility, adaptability, and reusability, giving rise to a "SERS-on-the-fly" sensing modality. By embedding chemical perception within a controllable robotic body, ASC-PR overcomes the longstanding limitations of static and passive SERS probes, establishing a new paradigm for localized, retrievable, and dynamically reconfigurable chemical sensing in complex biological environments.

Laser-conformal integration of plasmonic hot spots on magnetic soft robots

Realizing ASC-PR requires the integration of plasmonic sensing interfaces onto soft robotic bodies in a manner that is both spatially deterministic and mechanically compatible. Unlike planar substrates or post nanoparticle assembly strategies, plasmonic functionalization for ASC-PR must conform to curved and deformable surfaces while maintaining robust adhesion and uniform plasmonic activity under repeated magnetic actuation.

To meet these requirements, we employed femtosecond-laser *in situ* direct writing for site-specific and conformal fabrication of Ag/Pd alloy nanostructures on the surface of soft magnetic robots [Figure 2A]. A mixed precursor solution containing $AgNO_3$ and $PdCl_2$ was used [Supplementary Figure 2], and the tightly focused femtosecond laser induced localized photoreduction of Ag^+ and Pd^{2+} ions within the confined focal volume, enabling synchronous alloy formation and direct immobilization of plasmonic nanostructures on the deformable robotic body [Figure 2B]. This laser-based approach guarantees the intimate physical coupling between the plasmonic layer and the underlying elastomeric magnetic matrix [Supplementary Figure 3]. Conducted under ambient conditions, this approach allows precise on-demand patterning of plasmonic sensing unit [Figure 2C]. SEM images reveal densely packed Ag/Pd nanoparticles within the laser-written regions. AFM characterization further confirms nanoscale surface roughness and closely spaced interparticle features, which favor the formation of localized electromagnetic hot spots [Figure 2D]. Elemental analyses verify uniform Ag/Pd alloy formation across the patterned regions [Figure 2E and Supplementary Figure 4]. Time-of-flight secondary ion mass spectrometry (TOF-SIMS) depth profiling reveals a gradual transition from the plasmonic layer to the underlying substrate, with Ag/Pd signals decreasing and Si signal increasing with sputtering depth [Figure 2F]. Three-dimensional elemental reconstruction further confirms uniform coverage and intimate integration of the alloy with the soft substrate [Supplementary Figure 5].

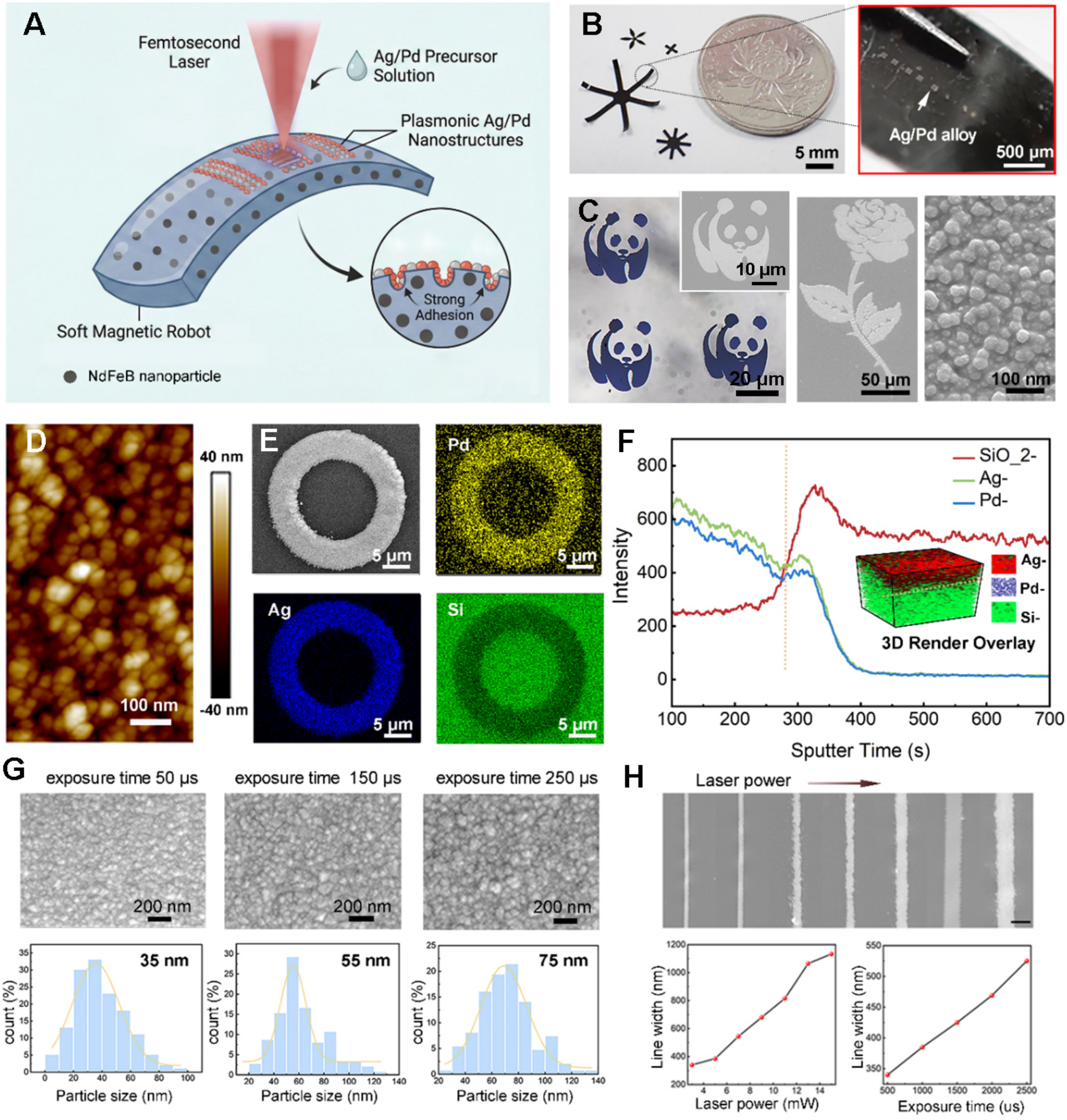

Figure 2. Site-specific and conformal fabrication of plasmonic nanostructures for ASC-PR. (A) Schematic of femtosecond laser *in situ* direct writing of Ag/Pd alloy nanostructures on the surface of a soft magnetic robot; (B) Optical images of soft magnetic milli-robots with Ag/Pd alloy patterns conformally integrated on curved surfaces; (C) SEM images of patterned Ag/Pd regions at different magnifications; (D) AFM characterization of Ag/Pd nanoparticles; (E) EDS elemental mapping of Ag/Pd patterns; (F) Depth profiling of Ag/Pd patterns on soft substrates (400 µm squares), with 3D reconstruction (inset); (G) Dependence of Ag/Pd nanoparticle size on single-point laser exposure duration; (H) Influence of laser power and exposure time on pattern linewidth, scale bar is 1µm. ASC-PR: Actuation-Sensing Coupled Plasmonic Robotics; SEM: scanning electron microscopy; AFM: atomic force microscopy; EDS: energy-dispersive X-ray spectroscopy.

Well-defined and tunable nanostructures are critical for enhancing the SERS performance of the milli-robots. Compared with nanosecond laser processing, femtosecond laser fabrication introduces negligible perturbation to the magnetization profiles of embedded NdFeB particles, preserving their structural and magnetic integrity [Supplementary Figure 6]. Notably, forming stable and high-resolution Ag/Pd alloy nanostructures is more challenging than that for single-metal systems. The threshold laser power for Pd deposition is generally higher than that for Ag [Supplementary Table 2 and Text 2], narrowing the processing window and potentially compromising pattern resolution. To balance alloy incorporation with pattern fidelity, a precursor molar ratio of 4:1 ($AgNO_3$:$PdCl_2$) was selected, yielding stable and reproducible patterns. Nanostructure morphology and pattern geometry can be deterministically tuned by adjusting laser power and exposure duration [Figure 2G and H], enabling precise control of sensing interfaces to meet diverse robotic operational requirements. Such controllable plasmonic architectures significantly enhance SERS activity, laying the foundation for high-sensitivity detection of trace biomolecules.

Plasmonic performance and chemical robustness of mobile Ag/Pd hot spots

The MagSense-Bot's plasmonic performance relies on surface nanostructures that provide strong, reliable SERS signals while maintaining chemical stability under repeated magnetic actuation and prolonged biological exposure. To this end, Ag/Pd alloy nanostructures were designed to balance plasmonic enhancement with chemical robustness, addressing the intrinsic instability of conventional Ag-based SERS substrates. The SERS enhancement arises from the synergistic combination of electromagnetic (EM) and chemical enhancement (CE) effects [Figure 3A]. Ag supports strong localized surface plasmon resonances, generating intense near-field confinement at interparticle gaps, whereas Pd modulates the interfacial electronic structure, facilitating charge-transfer interactions with adsorbed molecules and mitigating excessive hot-electron accumulation or localized heating. Therefore, the signal collected on Ag/Pd shows a broadened resonance response and a more spatially distributed enhancement [Figure 3B].

Crystal violet (CV) was used as a model Raman probe due to its well-defined vibrational fingerprints [Supplementary Table 3]. Comparative measurements reveal that Ag/Pd alloys produce significantly stronger and more reproducible SERS signals than pure Pd, while maintaining comparable spectral features to pure Ag [Figure 3C], with a detection limit difference of less than one order of magnitude [Supplementary Figure 7]. The sensitivity of the Ag/Pd-functionalized robots was further assessed by recording SERS spectra of CV across a concentrations range of 10^{-4} to 10^{-10} M [Figure 3D]. Characteristic Raman peaks remain clearly identifiable down to trace concentrations (10^{-10} M), and the corresponding calibration curve at 1,178 cm^{-1} exhibits a monotonic and concentration-dependent response [Figure 3E], demonstrating the capability of molecular-level detection. Spatial uniformity of the SERS response is particularly critical for mobile sensing interfaces, where the detection region continuously changes position and orientation. SERS signals from ten randomly selected locations on a single Ag/Pd-functionalized robot revealed a relative standard deviation of only 5.7% at 1,178 cm^{-1} [Figure 3F and G], indicating homogeneous plasmonic activity across the sensing surface. Beyond the spatial uniformity of a single device, the reproducibility of the femtosecond-laser-assisted fabrication strategy was further evaluated by independently fabricating five MagSense-Bots under identical processing conditions [Supplementary Figure 8]. Their SERS responses were evaluated using R6G as a probe molecule, and the intensity of a representative Raman peak was statistically analyzed. The devices exhibit highly consistent SERS responses with an relative standard deviation (RSD) of 7.2%, demonstrating reliable device-to-device reproducibility and the robustness of the fabrication process.

To quantitatively evaluate the signal amplification capability of the fabricated Ag/Pd nanostructures, the enhancement factor (EF) was calculated according to the standard[39]:

$$EF = \frac{I_{\mathrm{SERS}} \times N_{\mathrm{bulk}}}{N_{\mathrm{SERS}} \times I_{\mathrm{bulk}}} \tag{2}$$

where I_{SERS} and I_{bulk} represent the intensities of the same vibrational mode in the SERS and bulk Raman spectra, respectively. N_{SERS} is the number of molecules adsorbed on the substrate within the laser spot, and N_{bulk} is the number of molecules in the bulk sample that contributes to the SERS signals. Based on the experimental results, the EF value of Ag/Pd nanostructures was calculated to be about 2.5×10^8.

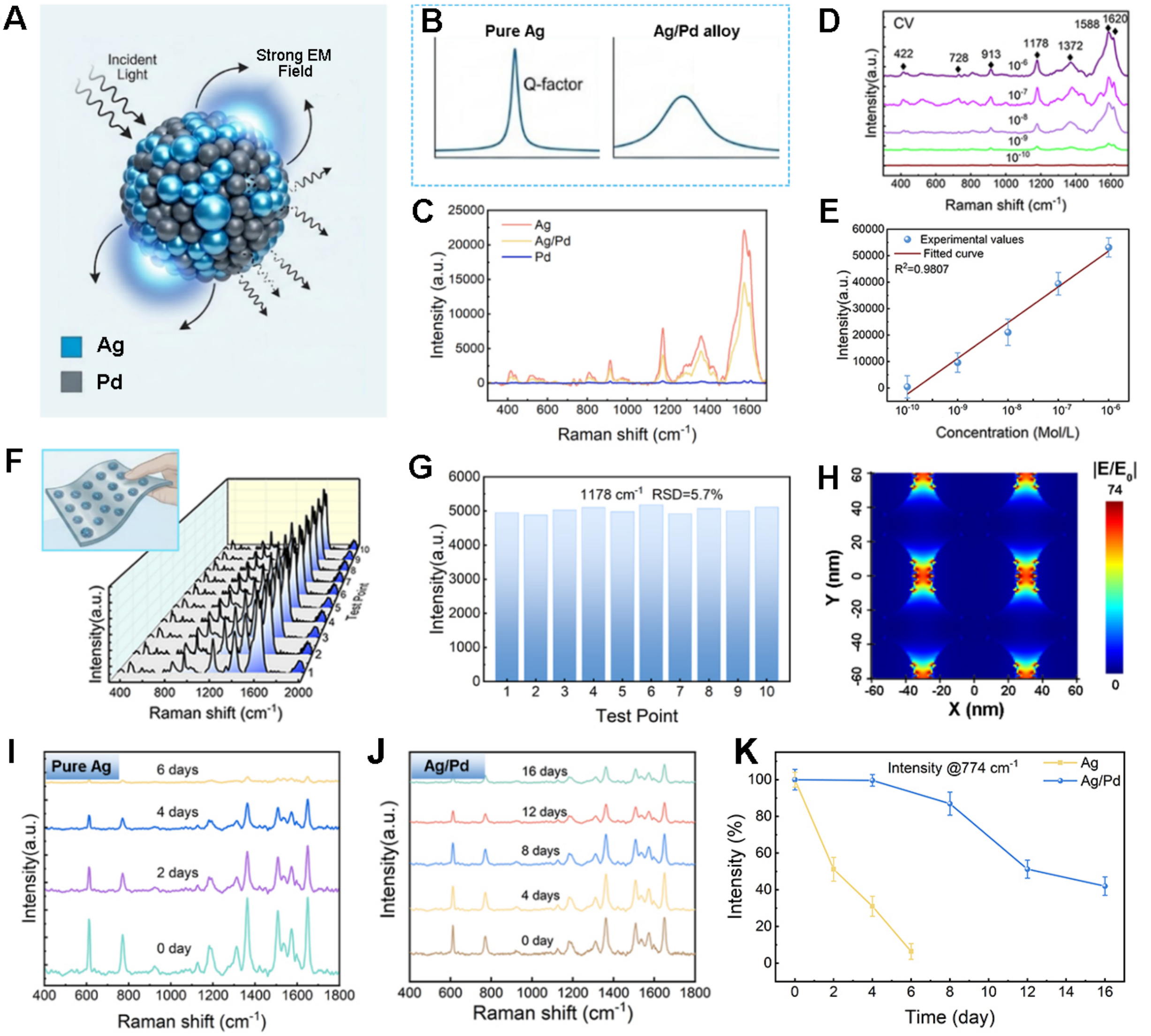

Figure 3. Plasmonic performance and chemical robustness of mobile Ag/Pd hot spots. (A) Schematic illustration of the SERS enhancement mechanism in Ag/Pd alloy nanostructures; (B) Conceptual illustration of plasmonic behavior in Ag/Pd alloys; (C) Comparison of SERS spectra acquired from pure Ag, Ag/Pd alloy, and pure Pd; (D) Representative SERS spectra of CV at different concentrations; (E) Corresponding calibration curve of Raman intensity at 1,178 cm^{-1} as a function of CV concentration; (F and G) Statistical analysis of SERS signal intensity from multiple locations on a single robot; (H) Local electric field distribution around Ag/Pd nanoparticles; (I) Time-dependent SERS signal evolution of pure Ag substrates; (J) Time-dependent SERS signal evolution of Ag/Pd alloy substrates; (K) Comparison of normalized SERS intensity decay at 774 cm^{-1} for pure Ag and Ag/Pd alloy substrates.Error bars represent the standard deviation (SD) of three repeated spectral intensity measurements collected from the same sample. EM: Electromagnetic; CV: crystal violet; RSD: relative standard deviation; SERS: surface-enhanced Raman scattering.

Finite-difference time-domain (FDTD) simulations further elucidate the near-field enhancement behavior of Ag/Pd nanostructures [Figure 3H]. The simulated electric field distribution shows pronounced localization at nanoscale interparticle gaps, consistent with the experimentally observed strong SERS signals. These results reflect the deterministic laser-based fabrication process and is essential for ensuring reliable signal interpretation during robotic motion.

Beyond sensitivity, long-term chemical robustness is an important factor for *in situ* and *in vivo* SERS sensing. Time-dependent measurements reveal that pure Ag nanostructures exhibit rapid signal degradation under ambient conditions (approximately 90% signal loss after 6 days), due to the surface oxidation and chemical

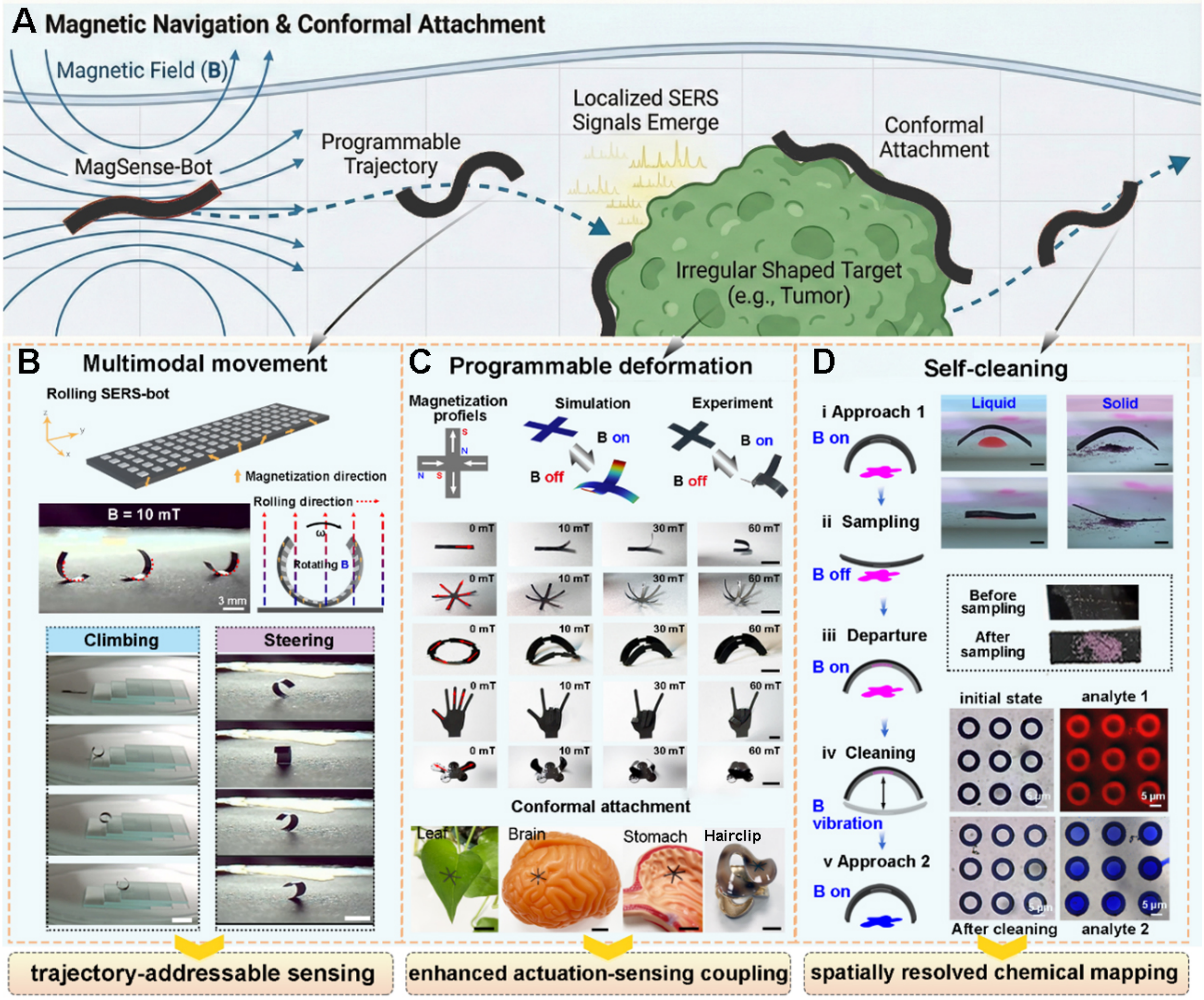

Figure 4. Magnetically enabled mobile SERS sensing through multimodal locomotion and programmable deformation. (A) Schematic illustration of the MagSense-Bot performing mobile SERS sensing; (B) Time-lapse optical images of multimodal locomotion of the magnetic robot, scale bar: 5mm; (C) Programmable deformation of the robot under magnetic actuation, scale bar 5 mm; (D) Schematic and experimental demonstration of a magnetically controlled sensing process. SERS: Surface-enhanced Raman scattering.

deterioration [Figure 3I]. In contrast, Ag/Pd alloy nanostructures maintain a substantially higher fraction of their initial SERS intensity over extended periods (about 20% signal attenuation after 6 days and 35% after 16 days) [Figure 3J]. A quantitative comparison of normalized SERS intensity decay at 774 cm^{-1} further highlights the superior stability of Ag/Pd hot spots relative to pure Ag [Figure 3K], underscoring the protective role of Pd in suppressing oxidative degradation. Therefore, the combination of Ag and Pd provide a favorable choice for implementing strong plasmonic enhancement, spatial uniformity, and chemical robustness, making them particularly well suited for mobile and repeatedly actuated SERS sensing within the ASC-PR framework.

Magnetically enabled multimodal locomotion and programmable deformation

Unlike static SERS substrates or passively dispersed nanoparticles, the MagSense-Bot integrates sensing functionality with programmable motion, allowing plasmonic hot spots to be actively delivered to regions of interest and operated through controlled magnetic fields [Figure 4A]. The magnetic robot body is fabricated from a composite of magnetic nanoparticles (NdFeB) and PDMS. By optimizing the NdFeB doping concentration, a balance between magnetic responsiveness and mechanical compliance can be achieved, enabling efficient magnetic actuation [Supplementary Figure 9 and Text 1]. When the mass fraction of NdFeB particles is 60%, the composite exhibits a magnetic strength of 81 emu/g and a Young's modulus of 1.23 MPa, providing optimal actuation performance.

When the MagSense-Bot incorporates a spatially varying (rotational) magnetization profile along its main body, it undergoes a field-induced curling configuration when subjected to a uniform magnetic field [Figure 4B]. This reconfiguration minimizes magnetic energy by aligning the local magnetization with the external field and establishes a mechanically stable rolling geometry. Under dynamic magnetic field actuation, the robot exhibits multimodal locomotion behaviors, including rolling, climbing and directional steering. As the external magnetic field rotates, the milli-robot continuously realigns its magnetic moment with the applied field, resulting in a stable and deterministic rolling motion. This rolling motion mechanism allows the robot to overcome step-like obstacles and surface discontinuities that are typically inaccessible to sliding or dragging motions. By modulating the orientation and rotation axis of the magnetic field, precise steering of the rolling direction is achieved, allowing programmable control over the locomotion path. The rolling velocity and steering accuracy governed by both the field magnitude and rotation frequency [Supplementary Figure 10]. Such mobility allows the sensing interface to be actively transported along predefined trajectories and to access spatially distributed targets. In contrast to the stochastic diffusion of free nanoparticles, this deterministic motion converts SERS detection from isolated, point-based measurements into a path-addressable sensing process, where both the spatial location and temporal sequence of chemical interrogation can be precisely defined.

Beyond translational motion, magnetic field modulation endows the MagSense-Bot with programmable deformation, transforming the plasmonic sensing surface from a passive coating into an actively adaptive interface [Figure 4C]. This deformation capability provides a critical mechanical pathway for improving interfacial contact, molecular capture efficiency, and sampling reliability during mobile SERS measurements. The programmable deformation arises from spatially encoded magnetization patterns within the soft robot body. By rationally coupling geometry with residual magnetization, a wide range of deterministic and reversible shape transformations can be achieved. Representative designs (such as cruciform, rectangular, gripper-like, ring-shaped, finger-inspired, and butterfly-like geometries) exhibit distinct deformation modes under uniform magnetic fields. A cruciform-shaped robot serves as a model system to illustrate the underlying mechanism [Supplementary Video 1]. When subjected to a uniform magnetic field (20 mT), adjacent arms magnetized with alternating N-S polarities experience opposing magnetic torques, driving symmetric out-of-plane bending and the formation of a stable three-dimensional configuration. Upon field removal, elastic recovery restores the original planar geometry, indicating highly reversible and repeatable deformation behavior consistent with simulation predictions. These magnetically programmed deformations are not merely geometric reconfigurations but directly enable deformation-assisted SERS sampling. By actively switching between planar and three-dimensional states, the robot can conformally adapt to uneven and curved surfaces, maximizing physical contact between plasmonic hot spots and target analytes. This conformal adaptability was validated across a variety of complex substrates, including biological tissues and anatomically relevant models, where intimate surface attachment could not be achieved using rigid or static SERS platforms. The structural stability of the surface metallic microstructures under pulsed magnetic fields was further evaluated. No noticeable morphological change was observed after repeated magnetic actuation [Supplementary Figure 11A and B]. Moreover, the SERS performance and actuation behavior remain stable after cyclic operation [Supplementary Figure 11C]. In addition, the microstructures remained firmly adhered to the substrate under a tensile strain of 50% applied to the flexible substrate [Supplementary Figure 11D and Video 2]. These results suggest that the plasmonic layer possesses sufficient mechanical robustness to withstand repeated deformation and actuation cycles during robotic locomotion.

Building upon these distinct magnetic actuation capabilities, dynamic magnetic control enables the coordinated temporal or parallel regulation of translational motion and structural deformation, thereby establishing a complete mobile sensing workflow [Figure 4D]. After targeted positioning, the robot undergoes deformation-assisted sampling at the site of interest, The sampling efficiency of the robot increases with bending deformation [Supplementary Figure 12]. Both SERS and fluorescence signals show stronger responses at larger bending angles, indicating enhanced molecular collection under deformation-assisted contact. Mechanically, this enhancement originates from larger elastic restoring torques generated in the robot's body during bending deformation, which increase the contact interaction at the sensing interface and facilitate molecular transfer to the plasmonic sensing surface. The bending torque of the beam-like structure can be expressed as[40]:

$$\tau = EIK \tag{3}$$

where E is the Young's modulus, I is the second moment of area, and k is the curvature. Since the curvature is approximately proportional to the bending angle, larger deformations produce greater elastic restoring torques, consistent with the observed trend. In addition, the number of attachment cycles also affects the sampling efficiency. Repeated contact between the robot and the target surface allows more analyte molecules to be collected and accumulated on the sensing surface. Consequently, the Raman signal intensity increases with the number of contact cycles until reaching a saturation state, where the sensing surface becomes fully occupied by adsorbed molecules [Supplementary Figure 13A and B].

Subsequently, the robot is actively withdrawn and exposed to high-frequency magnetic excitation. The resulting oscillatory motion induces controlled vibration of the robot body, facilitating desorption of previously adsorbed molecules and effectively regenerating the clean plasmonic surface. The desorption efficiency (η) is defined to quantify the effectiveness of this regeneration process, which represents the percentage of molecules removed from the plasmonic surface after magnetic oscillation. It can be calculated using the following equation:

$$\eta = \left(1 - \frac{I_{\text{before}}}{I_{\text{after}}}\right) \times 100\% \tag{4}$$

where I_{before} and I_{after} denote the intensity of the characteristic Raman peak before and after the magnetic oscillation process, respectively.

The experimental results show that the η is influenced by both the oscillation frequency of the magnetic field and the actuation duration [Supplementary Figure 13C]. A higher magnetic field frequency produces stronger and more frequent mechanical vibrations of the robot body, thereby enhancing molecular detachment from the plasmonic surface. Similarly, increasing the oscillation time allows more adsorbed molecules to be gradually released. As a result, the η increases with both frequency and actuation time, and can exceed 95% under optimized conditions, demonstrating effective regeneration of the sensing surface for repeated sensing cycles [Supplementary Figure 13D].

Subsequent re-positioning enables repeated sampling using the same robotic probe, eliminating the need for redeployment or probe replacement. By tuning the magnetic field parameters, the robot can reversibly transition between curled and extended configurations, allowing efficient sampling of both liquid and particulate analytes. Through the integration of controlled transport, adaptive deformation, and active surface renewal, magnetic actuation becomes an intrinsic component of the sensing strategy rather than a mere locomotion tool. This workflow underpins the concept of mobile and repeatable SERS sensing, establishing a practical route toward localized, on-demand chemical interrogation in confined and structurally complex environments.

Magnetically enabled “hot-spots-on-the-fly” for mobile and localized SERS sensing

Building upon the magnetic actuation capabilities that enable multimodal locomotion, programmable deformation, and vibration-assisted surface renewal, we demonstrate a representative *in situ* sensing scenario that captures the full potential of the “hot-spots-on-the-fly” concept. Specifically, the MagSense-Bot was deployed within a confined and geometrically heterogeneous workspace containing sharp turns, serpentine paths, and step-like height variations [Figure 5A and Supplementary Figure 14], mimicking realistic microenvironments encountered in biomedical and microfluidic contexts [Supplementary Video 3]. Two chemically distinct analytes, R6G and CV, were spatially separated and randomly distributed along the channel, in order to validate the localized and sequential SERS sensing. Under dynamic magnetic actuation, the MagSense-Bot navigated the complex pathway through controlled rolling and steering motions, actively transporting its plasmonic hot spots to designated locations [Figure 5B]. This mobility transforms SERS substrates from static detection platforms into actively repositionable sensing interfaces.

The entire sensing process follows a tightly coupled actuation-sensing workflow [Figure 5C], in which distinct magnetic field modes are temporally programmed to synchronize motion, conformal contact, signal acquisition, and surface renewal. The robot first rolling and steering towards the first sampling site containing R6G molecules. Then the robot altered its working mode from translational motion to deformation-assisted contact motion, where pulsed magnetic fields were applied to repeatedly drive conformal attachment between the plasmonic surface and the substrate. As shown in Figure 5D and E, SERS signals progressively enhanced along with the increasing number of pulsed contact cycles, indicating cumulative molecular adsorption facilitated by repeated deformation-enabled contact. This phenomenon highlights how magnetic actuation modulates sampling efficiency rather than merely positioning the sensor.

After the detection of Analyte 1-R6G, the robot was actively withdrawn and the subjected to an oscillating magnetic field (50 Hz, 10 mT). The high-frequency changing magnetic field vibrates the robot’s body, effectively promoting molecular desorption from the plasmonic surface. Time-resolved measurements [Figure 5F and G] reveal a monotonic decrease in R6G signal intensity with increasing oscillation duration, confirming that surface-bound molecules can be efficiently removed through magnetically induced vibration. The MagSense-Bot continued navigating forward to the second sampling site containing CV molecules. *In situ* SERS spectra acquired at this location exhibit only the characteristic Raman peaks of CV, with no detectable residual R6G signatures [Figure 5H and I]. This result demonstrates that the vibration-enabled cleaning process prevents cross-contamination between sequential measurements, enabling site-specific, multi-analyte sensing within a single deployment. As we can see, magnetic actuation not only governs robot locomotion but also dynamically promotes sensing performance, surface renewal, and re-sensing in a continuous and programmable manner. By integrating rotating, pulsing, and oscillating magnetic fields into a unified workflow, the MagSense-Bot achieves a spatially addressable, contamination-free chemical sensing strategy in confined and heterogeneous environments.

Stability and biomedical feasibility of magnetically mobile plasmonic sensing

For mobile plasmonic sensing to be practically deployable in biomedical settings, the sensing platform must sustain simultaneous mechanical actuation, chemical stability, and spectral reliability under complex physiological conditions. Unlike conventional static SERS substrates, the MagSense-Bot is designed to operate while continuously navigating, contacting, vibrating, and detaching within confined fluidic environments, placing stringent demands on its material robustness and functional integrity. We first conducted locomotion and deformation-assisted sampling experiments on freshly excised porcine gastric tissue [Supplementary Video 4], representing a compliant, curved, and mucus-covered organ surface [Figure 6A]. Despite the highly compliant and viscoelastic nature of the gastric tissue, the robot maintained stable rolling locomotion under rotating magnetic fields and could be guided toward a predefined sampling region

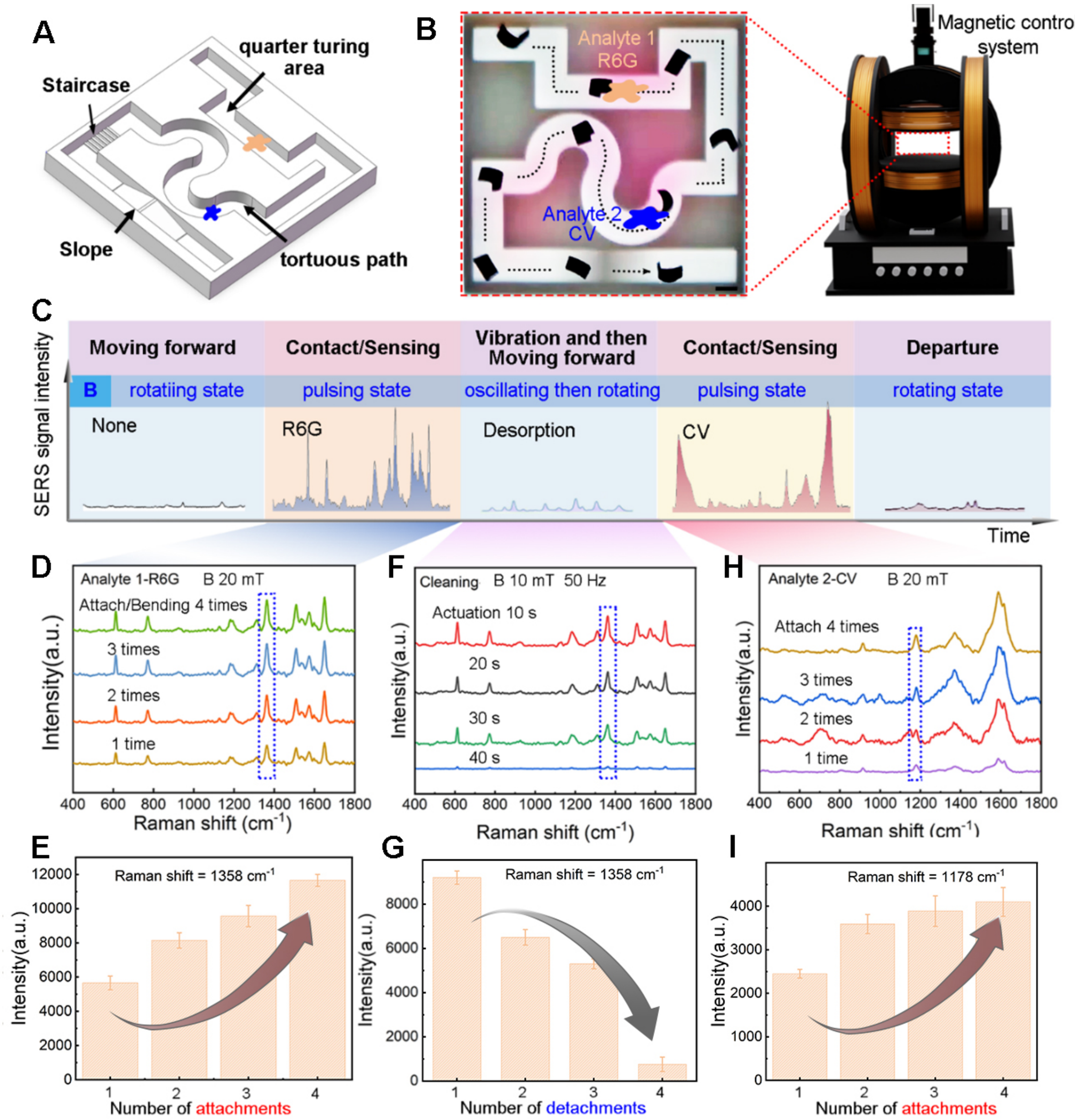

Figure 5. Magnetically enabled "hot-spots-on-the-fly" SERS sensing in a confined and heterogeneous environment. (A) Schematic illustration of a confined microenvironment with spatially separated analyte regions; (B) Demonstration of mobile and localized SERS sensing, scale bar 3mm; (C) Schematic of the actuation-sensing workflow of the MagSense-Bot; (D) SERS signal evolution of R6G and its intensity variation of the prominent peaks 1,358 cm^{-1} as a function of repeated deformation-assisted contact cycles (E); (F and G) Time-dependent desorption of R6G molecules under oscillating magnetic fields (50 Hz, 10 mT); (H and I) *In situ* SERS spectra acquired at the second sampling site, revealing characteristic CV peaks without residual R6G signatures. Error bars represent the standard deviation (SD) of three repeated spectral intensity measurements collected from the same sample. CV: Crystal violet; SERS: surface-enhanced Raman scattering.

along a controlled trajectory. Programmable structural deformation enabled the robot to transition from a three-dimensional curled state to a planar configuration, allowing the plasmonic sensing interface to conformally attach to the uneven tissue surface and efficiently collect molecules [Figure 6B]. After sampling, the robot reconfigures through a sequence of unfolding and rolling motions, allowing it to disengage from the sampling region and navigate back along the gastric surface [Figure 6C]. To further evaluate its stability under physiologically relevant conditions, the MagSense-Bot was immersed in representative biological fluids, including artificial cerebrospinal fluid (aCSF), simulated intestinal fluid (SIF), simulated gastric fluid (SGF), and artificial blood (AB) [Figure 6D]. After continuous immersion for up to 72 h, the robot exhibited no observable degradation in structural morphology, magnetic properties or laser-integrated plasmonic pattern fidelity [Figure 6E and Supplementary Figure 15 and 16A]. In addition, the microrobots exhibit stable actuation performance over repeated cycles [Supplementary Figure 16B] and after long-term storage (up to six months) [Supplementary Figure 16C], demonstrating good durability of the system. Inductively coupled plasma mass spectrometry (ICP-MS) further confirmed negligible Nd^{3+} ion release from the magnetic body, with a concentration of only 0.58 ppb after four days of immersion, which is well below the safety limits defined by the FDA and WHO (5 ppb) [Supplementary Figure 17]. This minimal leakage is attributed to the effective encapsulation of NdFeB nanoparticles within the silica gel matrix, underscoring the suitability of the soft magnetic body and the Ag/Pd plasmonic layer for prolonged exposure to biologically relevant fluids.

Beyond passive stability, we next examined whether the MagSense-Bot could function as an actively delivered, *in situ* chemical sensor within a clinically relevant scenario. Doxorubicin (DOX), a widely used chemotherapeutic agent with a narrow therapeutic window and dose-dependent systemic toxicity, was selected as a model analyte[41-44]. While systemic pharmacokinetic measurements based on blood sampling remain the clinical standard, they cannot capture the spatially heterogeneous drug distribution within tumor microenvironments. By contrast, magnetic navigation enables the MagSense-Bot to be precisely delivered to designated regions, where it establishes conformal contact with the local tissue environment and performs localized SERS interrogation [Figure 6F]. Using hepatocellular carcinoma cells (HepG2, purchased from Beyotime Biotechnology, Shanghai, China) treated with varying concentrations of DOX as a proof-of-concept model [Figure 6G], the MagSense-Bot successfully acquired distinct and concentration-dependent Raman signatures across a broad dynamic range [Figure 6H and I], with a detection limit reaching 10^{-10} M. For mobile *in situ* sensing, chemical robustness and signal stability become more critical than ultimate sensitivity, as the sensing surface is continuously exposed to complex biochemical environments. In this context, the incorporation of Pd into the Ag/Pd alloy plays a decisive role by suppressing silver oxidation and surface degradation, thereby preserving plasmonic activity during extended sensing operations.

To further demonstrate targeted sensing under dynamic conditions, we implemented a vascularized tumor-mimicking model in which the MagSense-Bot was magnetically navigated to regions surrounding liver cancer cells pretreated with different DOX concentrations [Figure 6J and K and Supplementary Video 5]. The robot enabled site-specific sampling within the confined vascular geometry, and spatially resolved SERS spectra collected from ten randomly selected locations revealed pronounced chemical heterogeneity in the local microenvironment [Figure 6L]. The results highlight the ability of the MagSense-Bot to perform mobile, localized, and repeatable chemical interrogation, rather than relying on a single static sensing site. The biocompatibility of the MagSense-Bot was evaluated using fibroblast cell cultures. Cells incubated with Ag/Pd-functionalized robots exhibited normal adhesion, spreading, and morphology comparable to untreated controls [Figure 6M], indicating negligible cytotoxic effects under the tested conditions. Therefore, the MagSense-Bot integrates magnetic actuation, plasmonic sensing, and material stability into a unified platform that is compatible with biologically relevant environments, paving the way toward on-demand, mobile SERS sensing of chemical microenvironments in living systems.

CONCLUSIONS

In this work, we present the MagSense-Bot, a magnetically actuated plasmonic robot that integrates active locomotion, programmable deformation, and robust SERS sensing into a single mobile platform. By coupling dynamic magnetic actuation with laser-integrated Ag/Pd plasmonic architectures, the system enables

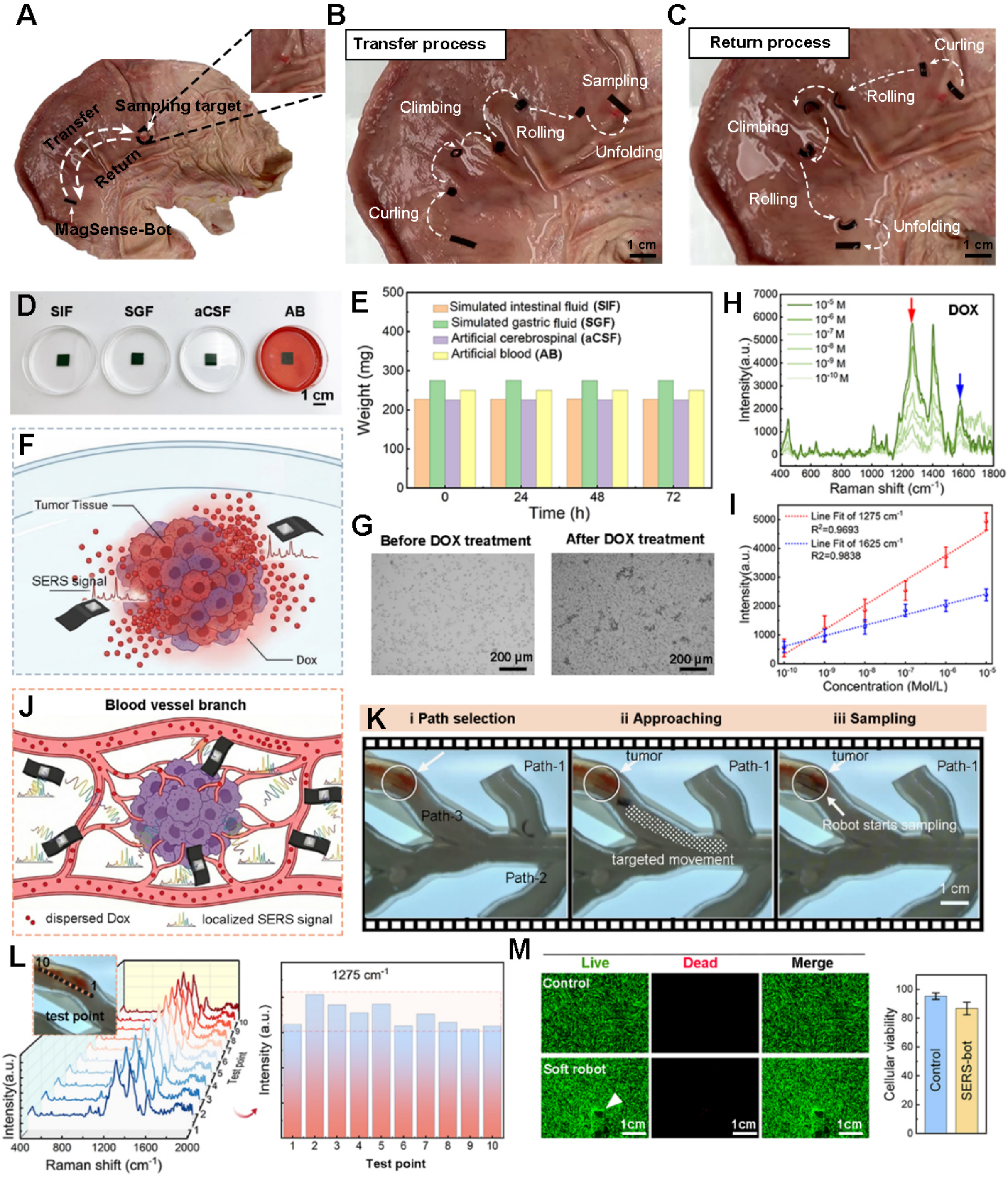

Figure 6. Stability, biocompatibility, and *in situ* feasibility of the MagSense-Bot for mobile SERS sensing in biologically relevant environments. (A-C) Deformation-assisted locomotion and surface sampling of the MagSense-Bot on *ex vivo* porcine gastric tissue; (D) Schematic illustration of the MagSense-Bot in representative physiological environments; (E) Weight changes of the MagSense-Bot after prolonged immersion (up to 72 h); (F) Schematic of magnetically guided delivery and conformal contact in a tumor-mimicking environment; (G) Microscopic images of HepG2 (purchased from Beyotime Biotechnology, Shanghai, China) cells treated before and after DOX at a concentration of 10^{-6}M; (H) Representative SERS spectra acquired by the MagSense-Bot at varying DOX concentrations; (I) Evolution of the signals at 1,275 and 1,625 cm^{-1} for the DOX with different concentrations. Error bars represent the standard deviation (SD) of three repeated spectral intensity measurements collected from the same sample; (J) Schematic illustration of targeted navigation and localized SERS sampling; (K) Time-lapse snapshots extracted from video recordings; (L) Spatially resolved SERS spectra collected from ten randomly selected locations; (M) Cell viability assessment after incubation with functionalized MagSense-Bots. Data are presented as mean ± SD. Error bars represent standard deviation. SIF: Simulated intestinal fluid; SGF: simulated gastric fluid; aCSF: artificial cerebrospinal fluid; AB: artificial blood; SERS: surface-enhanced Raman scattering; DOX: doxorubicin.

on-demand sensing beyond the limitations of conventional static SERS substrates. Magnetic field modulation endows the robot with multiple functional modes, including multimodal navigation in confined geometries, deformation-assisted conformal contact for reliable sampling, and high-frequency vibration for surface renewal and re-sensing. These capabilities establish robotic actuation as an integral component of the sensing strategy rather than merely a means of transport. The system further demonstrates robust structural and plasmonic stability under representative physiological conditions and enables targeted *in situ* detection of chemotherapeutic agents in tumor-mimicking microenvironments.

By bridging magnetic robotics with plasmonic spectroscopy, this work introduces a general framework for actuation-sensing-material co-design in mobile chemical sensing and creates new opportunities for on-demand biochemical interrogation in confined and dynamic biological environments, laying the groundwork for future autonomous robotic platforms with spatially resolved molecular diagnostic functions.

DECLARATIONS

Authors' contributions

Writing-original draft preparation: Li, R.
Partial experimental measurements: He, R; Zhou, Y; Luo, Z; Du, Y.
Experimental analysis planning: Wang, J; Zhu, Y.
Experimental scheme design and manuscript revision: Han, B; Ma, Z.-C.
Experimental implementation guidance, and manuscript revision: Wang, H.
All authors have read the manuscript and approved the final version.

Availability of data and materials

All data are available in the main text or the Supplementary Materials. Further information can be obtained from the corresponding authors upon reasonable request.

AI and AI-assisted tools statement

Not applicable.

Financial support and sponsorship

This work was supported by the National Natural Science Foundation of China (NSFC) under Grant Nos 62375168, 62575177, the Fundamental Research Funds for the Central Universities (YG2024QNA25, YG2024QNB19), the Shanghai Pilot Program for Basic Research Shanghai Jiao Tong University (No. 21TQ1400203), and the State Key Laboratory of Advanced Fiber Materials (Donghua University) (KF2514).

Conflicts of interest

All authors declared that there are no conflicts of interest.

Ethical approval and consent to participate

Not applicable.

Consent for publication

Not applicable.

Copyright

Supplementary Materials

Supplementary Materials

REFERENCES

1. Bi, X.; Czajkowsky, D. M.; Shao, Z.; Ye, J. Digital colloid-enhanced Raman spectroscopy by single-molecule counting. *Nature* **2024**, *628*, 771-5. DOI

2. Sharma, B.; Frontiera, R. R.; Henry, A.; Ringe, E.; Van Duyne, R. P. SERS: materials, applications, and the future. *Mater. Today.* **2012**, *15*, 16-25. DOI
3. Xue, M.; Zhang, W.; Jin, H.; et al. Composite additive manufacturing for suspended microelectrode arrays: advancing oriented myocardial tissue culturing and electrophysiological sensing. *Biosens. Bioelectron.* **2025**, *287*, 117686. DOI
4. Ding, Z.; Gu, T.; Zhang, R.; et al. Plasma-oxidized 2D MXenes subnanochannel membrane for high-performance osmotic energy conversion. *Carbon. Energy.* **2024**, *6*, e509. DOI
5. Wang, Y.; Jin, D.; Liu, X.; et al. Magnetic microrobot with drilling-sensing dual functionality for targeted biopsy of deep-seated tracheal microlesions. *Adv. Mater.* **2025**, *38*, e14664. DOI
6. Becerril-Castro, I. B.; Salgueiriño, V.; Correa-Duarte, M. A.; Alvarez-Puebla, R. A. Nano/Micromotor-driven SERS for highly sensitive and spatially controlled sensing. *Adv. Funct. Mater.* **2023**, *34*, 2314084. DOI
7. Bin, F.; Wu, X.; Liu, J.; et al. Micropattern of core-shell Ag@MCS/PEGDA nanoparticles fabricated by femtosecond laser maskless optical projection lithography. *Int. J. Extrem. Manuf.* **2025**, *7*, 035001. DOI
8. Xia, L.; Yang, Z.; Yin, S.; Guo, W.; Du, J.; Du, C. Hole arrayed metal-insulator-metal structure for surface enhanced Raman scattering by self-assembling polystyrene spheres. *Front. Phys.* **2013**, *9*, 64-8. DOI
9. Jalali, M.; Yu, Y.; Xu, K.; et al. Stacking of colors in exfoliable plasmonic superlattices. *Nanoscale* **2016**, *8*, 18228-34. DOI
10. Yang, H.; Guan, X.; Pang, G.; et al. Femtosecond laser patterned superhydrophobic/hydrophobic SERS sensors for rapid positioning ultratrace detection. *Opt. Express.* **2021**, *29*, 16904. DOI
11. Zhang, C.; Song, H.; Zeng, J.; et al. Ingestible electronic capsules for *in situ* sensing of diverse biomarkers. *Device* **2025**, *3*, 100935. DOI
12. Wang, X.; Zhu, L.; Qian, J.; et al. Atomic layer deposition assisted fabrication of insertable silver dendrites-based SERS substrates with high adhesion. *Appl. Surf. Sci.* **2023**, *640*, 158466. DOI
13. Chen, Y.; Pan, R.; Wang, Y.; et al. Carbon helical nanorobots capable of cell membrane penetration for single cell targeted SERS bio-sensing and photothermal cancer therapy. *Adv. Funct. Mater.* **2022**, *32*, 2200600. DOI
14. Qiu, G.; Liu, L.; Wang, D.; et al. Thermoplasmonic regulation and *in situ* detection of biomolecules with a photothermal-enhanced plasmonic biosensing system. *ACS. Nano.* **2025**, *19*, 16706-17. DOI
15. Hu, Y.; Hu, Y.; Wang, Z.; et al. Efficient concentration of trace analyte with ordered hotspot construction for a robust and sensitive SERS platform. *Int. J. Extrem. Manuf.* **2024**, *6*, 035505. DOI
16. Fan, S.; Scarpitti, B. T.; Smith, A. E.; Luo, Z.; Ye, J.; Schultz, Z. D. Linker-free synthesis of core/satellite nanoparticles for single-particle surface-enhanced Raman spectroscopy and photocatalysis. *Nano. Lett.* **2025**, *25*, 7785-92. DOI PubMed PMC
17. Zhang, Z.; Zhang, Z.; Hou, J.; et al. Stress-induced self-assembly of hierarchically twisted stripe arrays. *Science. Bulletin.* **2025**, *70*, 704-11. DOI
18. Dong, Y.; Wang, L.; Xia, N.; et al. Untethered small-scale magnetic soft robot with programmable magnetization and integrated multifunctional modules. *Sci. Adv.* **2022**, *8*, eabn8932. DOI PubMed PMC
19. Yang, J.; Zhang, Y.; Liu, Z.; et al. Magnetically actuated multimodal bioelectronic catheter for minimally invasive surgery and sensing. *Nat. Mater.* **2025**, *24*, 2019-31. DOI
20. Wang, B.; Shen, J.; Huang, C.; et al. Magnetically driven biohybrid blood hydrogel fibres for personalized intracranial tumour therapy under fluoroscopic tracking. *Nat. Biomed. Eng.* **2025**, *9*, 1471-85. DOI
21. Xie, R.; Han, F.; Yu, Q.; et al. A movable long-term implantable soft microfibre for dynamic bioelectronics. *Nature* **2025**, *645*, 648-55. DOI
22. Kim, Y.; Zhao, X. Magnetic soft materials and robots. *Chem. Rev.* **2022**, *122*, 5317-64. DOI PubMed PMC
23. Liu, X.; Wang, L.; Xiang, Y.; et al. Magnetic soft microfiberbots for robotic embolization. *Sci. Robot.* **2024**, *9*, eadh2479. DOI
24. Chen, Z.; Wang, Y.; Chen, H.; et al. A magnetic multi-layer soft robot for on-demand targeted adhesion. *Nat. Commun.* **2024**, *15*, 644. DOI PubMed PMC
25. Soon, R. H.; Yin, Z.; Dogan, M. A.; et al. Pangolin-inspired untethered magnetic robot for on-demand biomedical heating applications. *Nat. Commun.* **2023**, *14*, 3320. DOI PubMed PMC
26. Xu, X.; Kim, K.; Fan, D. Tunable release of multiplex biochemicals by plasmonically active rotary nanomotors. *Angew. Chem.* **2015**, *127*, 2555-9. DOI
27. Liu, S.; Xu, D.; Chen, J.; Peng, N.; Ma, T.; Liang, F. Nanozymatic magnetic nanomotors for enhancing photothermal therapy and targeting intracellular SERS sensing. *Nanoscale* **2023**, *15*, 12944-53. DOI
28. Cialla-may, D.; Bonifacio, A.; Bocklitz, T.; et al. Biomedical SERS - the current state and future trends. *Chem. Soc. Rev.* **2024**, *53*, 8957-79. DOI
29. Park, M.; Kim, Y.; Kim, S.; Lim, J. Y. Ultra-sensitive, on-site pesticide detection for environmental and food safety monitoring using flexible cellulose nano fiber/Au nanorod@Ag SERS sensor. *J. Hazard. Mater.* **2025**, *487*, 137197. DOI

30. Liu, H.; Gao, X.; Xu, C.; Liu, D. SERS Tags for biomedical detection and bioimaging. *Theranostics* **2022**, *12*, 1870-903. DOI PubMed PMC
31. Mao, L.; Yang, P.; Tian, C.; et al. Magnetic steering continuum robot for transluminal procedures with programmable shape and functionalities. *Nat. Commun.* **2024**, *15*, 3759. DOI PubMed PMC
32. Zhu, C.; Zhang, L.; Yang, Y.; et al. Light-driven liquid crystal elastomer actuators based on surface plasmon resonance for soft robots. *ACS. Appl. Mater. Interfaces.* **2024**, *16*, 69858-69. DOI
33. Xu, R.; Wang, X.; Chen, Y.; Tam, L. M.; Xu, Q. Bio-inspired magnetic soft robots with omnidirectional climbing for multifunctional biomedical applications. *Int. J. Extrem. Manuf.* **2025**, *8*, 015502. DOI
34. Liu, S.; Hou, Z.; Lin, L.; et al. 3D nanoprinting of semiconductor quantum dots by photoexcitation-induced chemical bonding. *Science* **2022**, *377*, 1112-6. DOI
35. He, Y.; Zhu, L.; Liu, Y.; et al. Femtosecond laser direct writing of flexible all-reduced graphene oxide FET. *IEEE. Photon. Technol. Lett.* **2016**, *28*, 1996-9. DOI
36. Zhang, Z.; He, R.; Han, B.; et al. Magnetically switchable adhesive millirobots for universal manipulation in both air and water. *Adv. Mater.* **2025**, *37*, 2420045. DOI
37. Johnson, P. B.; Christy, R. W. Optical constants of the noble metals. *Phys. Rev. B.* **1972**, *6*, 4370-9. DOI
38. Kelly, K. L.; Coronado, E.; Zhao, L. L.; Schatz, G. C. The optical properties of metal nanoparticles: the influence of size, shape, and dielectric environment. *J. Phys. Chem. B.* **2002**, *107*, 668-77. DOI
39. Schlücker, S. Surface-enhanced Raman spectroscopy: concepts and chemical applications. *Angew. Chem. Int. Ed.* **2014**, *53*, 4756-95. DOI
40. Öchsner, A., Makvandi, R. Euler-Bernoulli Beams and Frames. In *Finite Elements Using Maxima*; Springer International Publishing, 2019; pp 79-161. DOI
41. Cheng, Y.; Ji, Y.; Tong, J. Triple stimuli-responsive supramolecular nanoassembly with mitochondrial targetability for chemophotothermal therapy. *J. Controlled. Release.* **2020**, *327*, 35-49. DOI
42. Wallace, K. B.; Sardão, V. A.; Oliveira, P. J. Mitochondrial determinants of doxorubicin-induced cardiomyopathy. *Circ. Res.* **2020**, *126*, 926-41. DOI
43. Green, P. S.; Leeuwenburgh, C. Mitochondrial dysfunction is an early indicator of doxorubicin-induced apoptosis. *BBA-Mol. Basis. Dis.* **2002**, *1588*, 94-101. DOI
44. Kullenberg, F.; Degerstedt, O.; Calitz, C.; et al. *In vitro* cell toxicity and intracellular uptake of doxorubicin exposed as a solution or liposomes: implications for treatment of hepatocellular carcinoma. *Cells* **2021**, *10*, 1717. DOI